Chinese Chemical Letters 32 (2021) 796–800

Contents lists available at ScienceDirect

Chinese Chemical Letters

journal homepage: www.elsevier.com/locate/cclet

Communication

Highly active Pd-Fe/α-Al_2O_3 catalyst with the bayberry tannin as chelating promoter for CO oxidative coupling to diethyl oxalate

Wei-Chao Xing, Ji-Min An, Jing Lv*, Faisal Irshad, Yu-Jun Zhao, Sheng-Ping Wang*, Xin-Bin Ma

Key Laboratory for Green Chemical Technology, School of Chemical Engineering and Technology, Tianjin University, Collaborative Innovation Center of Chemical Science and Engineering, Tianjin 300072, China

ARTICLE INFO

Article history:
Received 19 May 2020
Received in revised form 23 June 2020
Accepted 24 July 2020
Available online 25 July 2020

Keywords:
Bayberry tannin
Diethyl oxalate
Phenolic hydroxyl groups
Ethyl nitrite
Pd-Fe/α-Al_2O_3

ABSTRACT

A novel Pd-Fe/α-Al_2O_3 catalyst was synthesized by incipient-wetness impregnation method with bayberry tannin as chelating promoter and commercial hollow column Raschig ring α-Al_2O_3 as support for the synthesis of diethyl oxalate from CO and ethyl nitrite. A variety of characterization techniques including N_2 physical adsorption, optical microscopy, scanning electron microscopy and energy dispersive system (SEM-EDS), inductively coupled plasma optical emission spectroscopy (ICP-OES), X-ray diffraction (XRD), X-ray photoelectron spectroscopy (XPS), transmission electron microscopy (TEM), were employed to explore the relationship between the physicochemical properties and activity of catalysts. It indicated that a large number of phenolic hydroxyl groups in bayberry tannin can efficiently anchor the active component Pd, reduce the particle size and make the active Pd as a multi-ring distribution on the commercial α-Al_2O_3 support, which were beneficial to improve the catalytic activity for the production of diethyl oxalate from CO and ethyl nitrite. 0.3 wt% Pd-Fe/α-Al_2O_3 showed excellent catalytic activity and selectivity in a continuous flow, fixed-bed reactor with the loading amount of 10 mL catalysts. Under the mild reaction conditions, the space-time yield of diethyl oxalate was 978 $g\,L^{-1}\,h^{-1}$ and CO conversion was 44% with the selectivity to diethyl oxalate of 95.5%.

Diethyl oxalate (DEO) is widely utilized at industrial domains to synthesize a variety of significant fine chemicals, such as dyes, pharmaceuticals, solvents, extractants, various intermediates and ethylene glycol (EG) [1]. Because of high industrial and market demand of EG, the hydrogenation of dimethyl oxalate (DMO) to produce EG has been studied for almost several decades [2–6]. Commonly, DMO is in solid state at room temperature and atmospheric pressure. It is necessary to dissolve DMO in anhydrous methanol or heat DMO to liquid state when it is applied to the production of ethylene glycol. However, DEO is a liquid chemical at room temperature and convenient as raw material for the production of ethylene glycol by hydrogenation [7,8]. Thus, more and more attention has been paid on diethyl oxalate, especially on its synthesis.

Oxalic esters have been typically synthesized by esterify-cation of oxalic acid and alcohols. In 1960s, the method of CO oxidative coupling to oxalic esters was discovered by Fenton *et al.* [9], which was initially carried out in the liquid phase by using copper-based catalysts. Further, UBE Industries and Montedison Ltd. have successively developed a new process for the synthesis of oxalate ester in the gas phase [10]. In recent years, plenty of research was related to the oxidative coupling of CO to oxalate ester and carbonic ester including the selection of the supports, the preparation of the catalyst, the doping of the metal auxiliaries and the reaction mechanism [11–15]. Many studies believed that Pd/α-Al_2O_3 had the best catalytic performance for diethyl oxalate production, but the favorable distribution of active components on the catalysts haven't worked out. Although some studies indicated that the catalytic activity of the egg-shell type distribution of the active sites was better than that of the aggregated particles [16,17], the high dispersion of the active component Pd on the supports has not been resolved effectively. In addition, for the supported noble metal catalysts, it is of great significance to decrease the active loading, especially for the potential industrial application. In order to further improve the catalytic activity and decrease the loading of Pd from the point view of industrialization, there is a pressing need to prepare highly active Pd/α-Al_2O_3 catalyst with lower Pd loadings and higher Pd dispersion.

* Corresponding authors.
E-mail addresses: muddylj@tju.edu.cn (J. Lv), spwang@tju.edu.cn (S.-P. Wang).

https://doi.org/10.1016/j.cclet.2020.07.038
1001-8417/

Here, we report the Pd-Fe/α-Al_2O_3 catalyst with an ultra-low Pd loading synthesized by introducing bayberry tannin as chelating promoter and commercial hollow column Raschig ring α-Al_2O_3 as support for the synthesis of diethyl oxalate from CO and ethyl nitrite. The catalytic activity for diethyl oxalate production over Pd-Fe/α-Al_2O_3 catalyst was evaluated in a continuous flow, fixed-bed reactor with the loading amount of 10 mL catalysts. The effect of bayberry tannin on the Pd dispersion and catalytic performance of Pd-Fe/α-Al_2O_3 for diethyl oxalate production was investigated.

Two Pd-Fe/α-Al_2O_3 catalysts (denoted as C1 and C2) have been synthesized with commercial hollow column Raschig ring α-Al_2O_3 as support under the same conditions except that the catalyst C1 was obtained upon the addition of bayberry tannin as chelating promoter (see Supporting information for details). Catalytic test in the CO oxidative coupling to DEO was carried out in a continuous flow fixed-bed reactor with ethyl nitrite generating device (loading 10 mL Pd-Fe/α-Al_2O_3 catalyst). The catalytic performances of C1 and C2 were presented in Table 1. It is demonstrated that conversion of CO and the space-time yield (STY) of DEO of C1 was nearly twice that of C2. The selectivity to DEO for C1 and C2 were almost identical, but they increased greatly compared with previous study (89%) [16]. In addition, as shown in Table 1, for the C1 and C2, the theoretical Pd and Fe loading was 0.50 wt% while the actual Pd loading of C1 and C2 were 0.35 and 0.11 wt%, and the actual Fe loading of C1 and C2 were both 0.29 wt%, as shown in Table 1. The value of Fe: Pd of catalysts were about 1.2:1 and 1:2.6, determined by inductively coupled plasma optical emission spectrometer (ICP-OES). It was obvious that the bayberry tannin played a vital role in anchoring Pd on the support during the preparation process.

Fig. S2 (Supporting information) shows transmission electron microscopy (TEM) images of Pd nanoparticles in the impregnation solutions with and without bayberry tannin addition. It is obvious that in the presence of bayberry tannin, Pd nanoparticles can be uniformly dispersed (Fig. S2a), while Pd aggregated and grew in the absence of bayberry tannin, as shown in Fig. S2b. This is mainly because a large number of phenolic hydroxyl groups in bayberry tannin could chelate with the Pd and anchor the Pd metal ions to inhibit the agglomeration [18].

TEM images presented in Figs. 1a and b revealed that the Pd-NPs of C1 were highly dispersed on the α-Al_2O_3 support, while the Pd-NPs of C2 were somewhat aggregated into large nanoparticles during the catalyst preparation process. On the basis of the size distribution histograms shown in Figs. 1c and d, the average size of Pd-NPs of C1 was 4.8 nm, which was much smaller than that of C2 (7.3 nm). Moreover, for C1 catalyst, the size distribution of Pd-NPs became much narrower and uniform as compared with that of C2. In order to know about the state of Pd and Fe on this catalyst, high resolution TEM (HRTEM) was used to analyze and explain the significant performance of Pd-Fe/α-Al_2O_3. HRTEM images (Fig. 1e) of C1 catalyst presents a group of three nanoparticles (indicated as I, II and III) with different morphology and arrangement of atomic planes. Perpendicular lines were drawn (red color) to calculate the interplanar distances (IDs) in the micrographs, the average measure was compared with the JCPDS Cards. to identify the crystalline phase observed in the nanoparticle. In zone I, the average measure of the IDs was 0.228 ± 0.005 nm and matched the (111) plane of the Pd crystalline phase (JCPDS No. 04-46-1043) [19,20]. For zone II, the ID measure was 0.284 ± 0.004 nm and matched the (200) plane of $O_4Pd_{3.5}$ crystalline phase or the (111) plane of $Fe_{1-x}O$ crystalline phase (JCPDS No. 04-005-475) [21,22]. In zone III, the ID was calculated as 0.241 ± 0.005 nm, and matched the (111) plane of the $FePd_3$ crystalline phase (JCPDS No. 04-001-7354), which indicates the formation of a bimetallic Pd-Fe alloy. Meanwhile, Fig. 1f also detected the Pd-Fe alloy and Pd crystalline phase clearly. The presence of the bimetallic alloy of $FePd_3$ in the Pd-Fe/Al_2O_3 catalyst may produce a greater activity than monometallic Pd particles or simple mixture of Pd and Fe catalyst [22]. On the one hand, the bimetallic Pd alloy with a second metal such as Fe or Co as the catalytic sites have a higher electron density on Pd atoms, which is likely due to incomplete filling of the valence shell of the second metal and electron transfer to unoccupied Pd orbitals [23]. On the other hand, though the presence of Fe species leads to a decrease of chemically accessible Pd sites on the surface of catalyst, the Pd-Fe alloy generate a synergism effect favoring performance of a bimetallic catalyst [22]. This synergism effect is due to the electronic structure of the surface d-band in alloy sites of bimetallic catalysts, which makes them more active than monometallic catalysts [24,25].

In order to identify the spatial distribution of the active Pd on the commercial hollow column Raschig ring α-Al_2O_3 support, C1 and C2 were cut from the mid and the distribution of the active component Pd on the commercial hollow column α-Al_2O_3 support were observed with an optical microscope, as shown in Figs. 2a and b. It can be clearly seen that the active component Pd of C1 (Fig. 2a) with bayberry tannin addition distributed as a tree-ring. However, the Pd of C2 (Fig. 2b) without bayberry tannin addition appeared like an egg-shell, and the active component mainly gathered on the surface of the carrier, which was consistent with the previous report [26].

Meanwhile, scanning electron microscopy and energy dispersive system (SEM-EDS) was applied to better illustrate the distribution of Pd and Fe atoms on the catalysts. Figs. S5a and b (Supporting information) present the cross sectional images of C1 and C2 by using linear scanning to scan a half ring of the catalysts, respectively [16]. Note that the Pd atoms of C1 (Fig. S5a) with bayberry tannin addition showed multi-peak distribution, which had the characteristic of tree-ring distribution, as a whole. By contrast, the Pd atoms of C2 (Fig. S5b) without bayberry tannin addition showed single-peak distribution, which had the characteristic of egg-shell distribution, as a whole. This was consistent with the results of optical microscopy images. In addition, the Fe atoms distribution of C1 and C2 (Figs. S5a and b) were almost no strong peaks, which mean a uniform distribution on the catalysts.

A feasible multi-ring distribution mechanism of Pd nanoparticles of catalysts with the addition of bayberry tannin was proposed, as shown in Scheme 1. The Pd ions in the aqueous solution were anchored by the phenolic hydroxyl groups of bayberry tannin and a strongly bonded structure formed in the solution. During the impregnation process, the remaining phenolic hydroxyl groups can be also anchored to the support, which improve the strengthening interactions between the active component Pd and the support. Thus, the active component Pd impregnated into the hollow column Raschig ring structure of α-Al_2O_3 support. By heating at 500 °C, the bayberry tannin was decomposed into CO_2 with leaving a large amount of space field inside the carrier [12], and finally formed a multi-ring distribution. The tree-ring distribution of the Pd on commercial hollow column Raschig ring α-Al_2O_3 support made the higher dispersion of Pd and

Table 1
CO oxidative coupling to DEO on different catalysts.[a]

Catalysts	Pd content (wt%)	Fe content (wt%)	X_{CO} (%)	S_{DEO} (%)	STY_{DEO} ($g\,L^{-1}\,h^{-1}$)
C1[b]	0.35	0.29	33.6	95.5	729
C2[c]	0.11	0.29	16.5	96.0	424

[a] Reaction conditions: 10 mL of catalyst, 3000 h^{-1} of gas hourly space velocity (GHSV), reactants including 20% CO, 16% NO, 4% O_2, 60% N_2; 0.04 MPa, 130 °C.
[b] C1 was prepared with the addition of bayberry tannin.
[c] C2 was prepared without the addition of bayberry tannin.

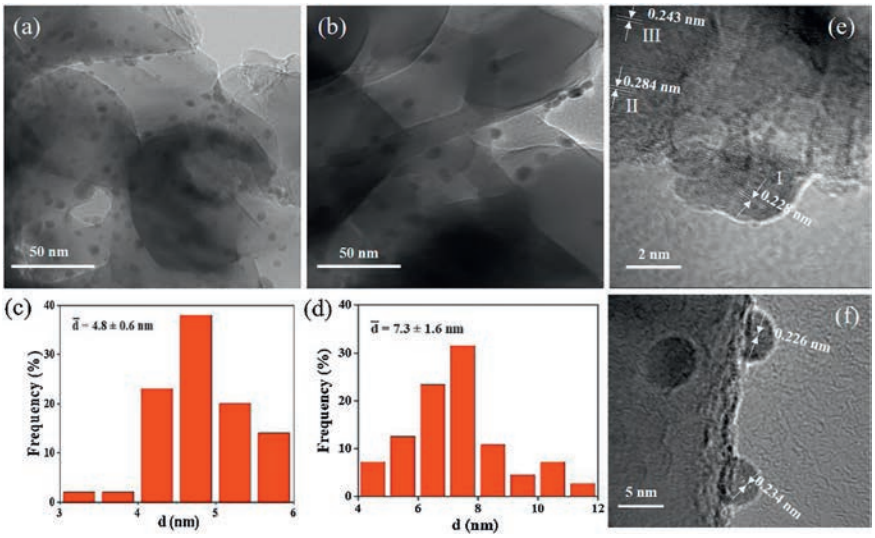

Fig. 1. TEM images of C1 (a) and C2 (b) with the corresponding size distributions of Pd NPs (c, d) and HRTEM images of C1 (e, f).

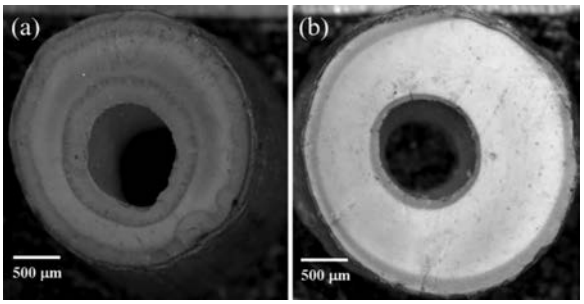

Fig. 2. Optical microscopy images of C1 (a) and C2 (b).

more space fields, which might be one of the reasons for the high activity of C1 catalyst.

It was well known that Pd can be easily reduced in a hydrogen atmosphere. Previous studies [16,17,27] revealed that Pd/α-Al_2O_3 catalyst had zero valence of Pd after reduction, however the analysis of the valence of Pd after the reaction was less explored. The X-ray photoelectron spectroscopy (XPS) characterizations for the Pd valence of C1 and C2 catalysts were carried out, and it was found that after 10 h of reaction, the valence of Pd was not all zero, which was consistent with the previous reports [16,27]. The valence of Pd changed between zero and divalent states during the stabilized reaction progress. However, by comparing the catalyst with and without bayberry tannin addition, as shown in Fig. 3a parts 1 and 2, it was found that, for the C1 catalyst with bayberry tannin addition, the binding energies of Pd $3d_{5/2}$ had a little right shift from 335.9 eV to 335.5 eV, meaning that the addition of bayberry tannin enhanced the interaction of Pd with α-Al_2O_3 support. Meanwhile, as shown in Fig. 3b parts 1 and 2, it is noted that the valence state of Fe was unchanged and remained the low-valence state. It indicated that there were some $Fe_{1-x}O$ (1-x is between 0.84−0.95) crystalline phase on the catalysts.

Furthermore, in order to investigate the influence of Pd loading on the CO oxidative coupling activity, a series of catalysts with the different Pd loadings (0.1 wt%, 0.3 wt%, 0.5 wt%, 0.7 wt%) were synthesized with the addition of 0.5 wt% bayberry tannin, the molar ratio of Pd to Fe in each catalyst was always 1:1. And the catalytic performances of a series of catalysts for DEO synthesis were presented in Table 2. It is noted that the conversion rate of CO and STY of DEO showed a volcanic change with the increase of Pd loading. When the Pd loading was 0.3 wt%, the conversion of CO was the highest, achieving 44 wt% with STY of DEO being 978 $g\,L^{-1}\,h^{-1}$. Under the conditions of low Pd loading up to 0.30 wt%, the catalyst activity rose with the increase of active sites. However, it was interesting to note that as the loading of Pd further increases, the activity of the catalyst decreases, which was most likely due to the accumulation of Pd in the presence of excessive Pd loading. Then, as shown in Table 2, along with the increment of Pd loading, the TOF values of the catalysts gradually diminished, however, the STY of DEO of the catalysts for the synthesis of diethyl oxalate firstly increased and then decreased. Note that when the Pd loading was 0.23 wt%, the STY of DEO reached the highest, and the TOF values of the catalysts was also relatively high. This indicated that 0.23 wt% Pd loading was an optimal content from both catalytic performance and economical points of view. In addition, note that the selectivity of DEO in these catalysts was almost equivalent (about 96%), which was mainly due to the absence of acid sites on the support [16]. A large amount of ethyl nitrite decomposition will produce more by-products in the presence of acid sites, which will seriously affect the selectivity of diethyl oxalate. Whereas, we used α-Al_2O_3 as support for the catalysts, and there were no acid sites on the surface of alumina calcined to 1200 °C, leading to the high selectivity of DEO.

TEM images and the Pd particle statistics of catalysts with the different Pd loadings were shown in Fig. S6 (Supporting information). It indicated that the average particle size of Pd was increased from 3.4 nm to 5.7 nm with the increase of Pd loading. Generally, the smaller Pd particles are favorable for the improvement of catalytic performance. However, for 0.1 wt% Pd-Fe/α-Al_2O_3, the active sites were insufficient, leading to the lower CO conversion and STY of DEO. It is noted that 0.3 wt% Pd-Fe/α-Al_2O_3 performed best due to the sufficient active sites and smaller Pd particles.

According to test of N_2 physical adsorption, it is easier to intuitively find that the microstructure of the catalysts was greatly affected by the Pd loading and bayberry tannin together (Fig. S9 and Table S3 in Supporting information). Compared with other Pd loading catalysts, specific surface area of 0.3 wt% Pd-Fe/α-Al_2O_3 increased from 10 m^2/g to 14 m^2/g. Large specific surface area was

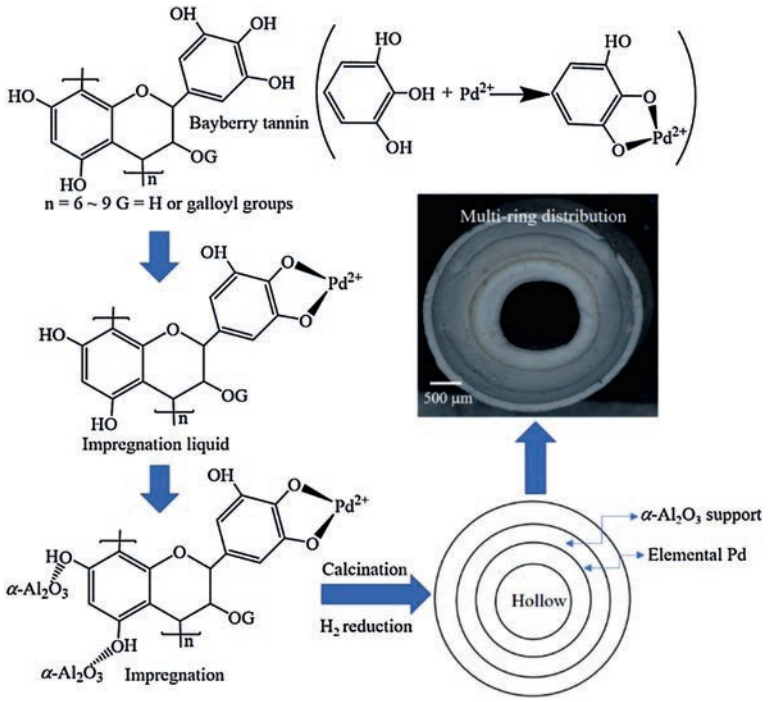

Scheme 1. Schematic diagram about the general synthetic procedures of Pd/α-Al_2O_3 with bayberry tannin.

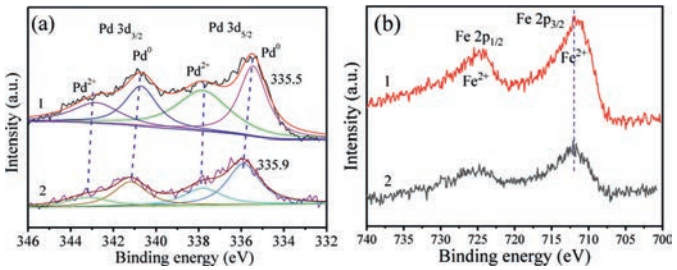

Fig. 3. Pd 3d (a, b) and Fe 2p (c, d) XPS spectra of C1 and C2.

Table 2
Catalytic activities, Pd content, Fe content, pore size and Pd dispersion of various catalysts for CO coupling to DEO.

Catalysts	Pd content [a] (wt%)	Fe content [a] (wt%)	D [b] (nm)	Pd dispersion [c] (%)	X_{CO} (%)	S_{DEO} (%)	STY_{DEO} (g L^{-1} h^{-1})	TOF values (h^{-1})
0.1Pd-Fe/α-Al_2O_3	0.085	0.075	3.4	30.1	26.5	96.6	572	1669
0.3Pd-Fe/α-Al_2O_3	0.23	0.22	3.9	25.0	44.0	95.5	978	1283
0.5Pd-Fe/α-Al_2O_3	0.35	0.29	4.8	22.4	33.8	95.6	729	699
0.7Pd-Fe/α-Al_2O_3	0.45	0.48	5.7	18.2	23.6	97.0	509	466

[a] Determined by ICP-OES.
[b] Particle size determined by TEM.
[c] Determined by TEM.

favorable for Pd dispersion, further accelerating the catalytic activity for DEO production.

The reaction mechanism (Scheme 2) of the gas-phase catalytic coupling of carbon monoxide to diethyl oxalate was surface-control reaction [27]. Ethyl nitrite was initially inserted into Pd to change zero-valent of Pd by continuously oxidization to divalent Pd. At the same time, the linear carbon monoxide adsorbed on the catalyst surface, resulting in an easy conversion to the divalent Pd alkane compound which formed a Pd carbonyl intermediate complex. Then Pd carbonyl compound was unstable. When there was sufficient space field (no steric hindrance), the bisethoxycarbonyl Pd on the catalyst surface can be eliminated to form diethyl oxalate. The divalent Pd was reduced to zero valent Pd and then entered to next round for cyclic catalytic process. The key to the smooth operation of this circulation system was not only to provide more space fields, but also to provide more reactive sites. For large-scale production of catalysts with commercial α-Al_2O_3 support, it was often difficult to improve the active sites dispersion. Here, the introduction of bayberry tannins as chelating promoter resulted in the reduction of particle size and the uniform dispersion of active Pd on the Pd-Fe/α-Al_2O_3 catalyst.

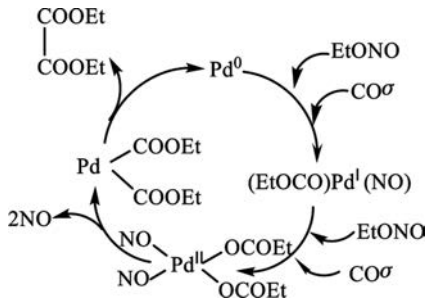

Scheme 2. Scheme of CO coupling reaction mechanism.

In this work, a novel Pd-Fe/α-Al_2O_3 catalyst with high activity was successfully synthesized by adding bayberry tannin as chelating promoter and commercial hollow column Raschig ring α-Al_2O_3 as support for CO oxidation coupling of ethyl nitrite to diethyl oxalate. A large number of phenolic hydroxyl groups in bayberry tannin can efficiently anchor the active component Pd, reduce the particle size and improve the dispersion of the active Pd. This kind of distribution provides enough space field more like a miniature reactor, which led to excellent catalytic activity. Due to simple preparation method, low Pd contents and high production yield rate, this highly active Pd-Fe/α-Al_2O_3 catalyst is favorable for industrial application potentiality. More importantly, this work should be universal for designing other supported precious metal industrial catalysts with maximum dispersion and smaller particle size of active species.

Declaration of competing interest

The authors declared that they have no conflicts of interest to this work.

Acknowledgment

Financial support by the National Key R&D Program of China (No. 2017YFB0307300) is gratefully acknowledged.

Appendix A. Supplementary data

Supplementary material related to this article can be found, in the online version, at doi:https://doi.org/10.1016/j.cclet.2020.07.038.

References

[1] H.Y. Song, R.H. Jin, M. Kang, et al., Chin. J. Catal. 34 (2013) 1035–1050.
[2] B.Y. Yu, I.L. Chien, Chem. Eng. Res. Des. 121 (2017) 173–190.
[3] Y.T. Liu, J. Ding, J.Y. Yang, et al., Catal. Commun. 98 (2017) 43–46.
[4] Y.J. Zhao, H.H. Zhang, Y. Xu, et al., J. Energy Chem. 49 (2020) 148–256.
[5] X.B. Yu, T.A. Vest, N.G. Boure, et al., J. Catal. 380 (2019) 289–296.
[6] C.C. Zhang, F. Yu, B. Dai, et al., Catal. Commun. 102 (2017) 31–34.
[7] J. Ding, T. Popa, J. Tang, et al., Appl. Catal. B: Environ. 209 (2017) 530–542.
[8] J. Ding, M.H. Fang, Q. Zhong, et al., Appl. Catal. B: Environ. 232 (2018) 348–354.
[9] D. M. Fenton, P. J. Steinwand, PCT/US1967/3393136, 1967.
[10] H. Miyazaki, Y. Shiomi, S. Fujitus et al., PCT/US1983/4410722, 1983.
[11] S.Y. Peng, Z.N. Xu, Q.S. Chen, et al., ACS Catal. 5 (2015) 4410–4417.
[12] S. Peng, Z. Xu, Q. Chen, et al., Chem. Commun. 49 (2013) 5718–5720.
[13] E. Leino, N. Kumar, P. Arvela, et al., Catal. Today 306 (2018) 128–137.
[14] G. Zhang, D. Zhao, J. Yan, et al., Appl. Catal. A: Gen. 579 (2019) 18–29.
[15] C. Murugan, H.C. Bajaj, Fuel Process. Technol. 92 (2011) 77–82.
[16] X. Gao, Y. Zhao, S. Wang, et al., Chem. Eng. Sci. 66 (2011) 3513–3522.
[17] X. Jiang, Y. Su, B. Lee, et al., Appl. Catal. A: Gen. 211 (2001) 47–51.
[18] X. Huang, H. Mao, X. Liao, et al., Catal. Commun. 12 (2011) 1000–1004.
[19] H. Bai, X. Fang, C. Peng, ACS Sustain. Chem. Eng. 7 (2019) 7700–7707.
[20] X. Zou, Z. Rui, H. Ji, ACS Catal. 7 (2017) 1615–1625.
[21] Y. Xiang, X. Li, C. Lu, et al., Appl. Catal. A: Gen. 375 (2010) 289–294.
[22] J.F. Yang, S.S. Li, L.L. Zhang, et al., Appl. Catal. B: Environ. 201 (2017) 266–277.
[23] I. Khalilov, I. Ilyasov, V. Shatilov, et al., Catal. Use Indium 5 (2013) 318–326.
[24] W. Yu, M.D. Porosoff, J.G. Chen, Chem. Rev. 112 (2012) 5780–5817.
[25] M. Lesiak, M. Binczarski, S. Karski, et al., J. Mol. Catal. A: Chem. 395 (2014) 337–348.
[26] X. Feng, L. Ling, Y. Cao, et al., J. Phys. Chem. C 122 (2018) 1169–1179.
[27] Z.H. Gao, Z.C. Liu, F. He, et al., J. Mole. Catal. A: Chem. 235 (2005) 143–149.